Generation of Novel Synthetic Portable Chest X-ray Images for the Automatic COVID-19 Screening

Daniel I. Morís

Centro de investigación CITIC, Universidade da Coruña, Spain

Grupo VARPA, Instituto de Investigación Biomédica de A Coruña (INIBIC), Universidade da Coruña, Spain

J. de Moura

Centro de investigación CITIC, Universidade da Coruña, Spain

Grupo VARPA, Instituto de Investigación Biomédica de A Coruña (INIBIC), Universidade da Coruña, Spain

J. Novo

Centro de investigación CITIC, Universidade da Coruña, Spain

Grupo VARPA, Instituto de Investigación Biomédica de A Coruña (INIBIC), Universidade da Coruña, Spain

M. Ortega

Centro de investigación CITIC, Universidade da Coruña, Spain

Grupo VARPA, Instituto de Investigación Biomédica de A Coruña (INIBIC), Universidade da Coruña, Spain

ABSTRACT

The diagnosis and the study of the evolution of the COVID-19 is crucial to tackle the challenge that this disease represents for the health care services. Chest X-ray imaging allows to visualize the pulmonary

regions, where the COVID-19 causes its main affectation, being very useful. In order to reduce the risk of cross-contamination, crucial aspect in the pandemic, portable chest X-ray devices are advantageous being easier to decontaminate in comparison with the fixed machinery, despite offering a lower image quality. Furthermore, the recent emergence of the COVID-19 implies a data scarcity that must be tackled. In this chapter, we present the analysis of a strategy that generates novel synthetic portable chest X-ray images using the CycleGAN, an architecture for image translation that is trained with unpaired data. The novel set of images is then added to the original dataset, improving the performance of the classification model.

Keywords: Computer-Aided Diagnosis, Deep Learning, Biomedical Imaging, Image Generation, CycleGAN, Image Translation, Computer Vision, Classification

INTRODUCTION

The COVID-19 is a pathology that can affect several parts of the body, while its main affectation is located on the respiratory tissues. The pathogen that causes this disease is known as SARS-CoV-2, a type of coronavirus, which is highly contagious, reason why it was rapidly spread worldwide forcing the World Health Organization to declare the COVID-19 as a global pandemic in 12th March 2020 (Ciotti et al., 2020). Currently, more than 242 million confirmed cases alongside more than 4.9 million deaths were reported worldwide (Coronavirus Resource Center, Johns Hopkins, 2020). There are several techniques to diagnose the COVID-19 but the gold-standard is the RT-PCR test (Tahamtan & Ardebili, 2020). However, it could be interesting for clinicians to have more information than the simple diagnostic provided by this technique. The main affectation of the COVID-19 is located in the pulmonary area and, therefore, chest X-ray imaging can be very useful to visualize this region to diagnose the pathology, to study its severity and to understand its evolution (Jacobi et al., 2020), as it has been widely used in the last decades to diagnose other typical pulmonary diseases and detect pathological structures as is the case, for example, of the pneumonia (Fiszman et al., 2000), the tuberculosis (Van Cleeff et al., 2005), the fibrosis (Puderbach et al., 2007) or the lung nodules (Wei et al., 2002). In the context of the COVID-19, this image modality can be used as a complement to the diagnostic result of the RT-PCR. With all these ideas into account, we can conclude that chest X-ray emerges as a powerful approach to visualize the affection of this pulmonary disease. Despite its lower quality in comparison with other advanced methods, as the Computerized Tomography (CT) (Hayden & Wrenn, 2009), the chest X-ray captures are easier and cheaper to perform. On the other hand, as the SARS-CoV-2 is easily spread, it is very important to decontaminate the capture devices. In the same way, many patients are bedridden and, therefore, it is impossible for them to move to the radiology room. To solve these problematics, radiologists are recommended to use portable chest X-ray devices instead of the fixed machinery (Kooraki et al., 2020), as this kind of devices are easier to decontaminate and can be moved to where the patient is placed. However, in some cases, clinicians could decide to use more advanced techniques that provide a more detailed visualization of the pulmonary regions if it is necessary, in order to have a more precise localization of the pathological structures, despite the higher cost and difficulty of the captures. This is the case of the CT, that provide a 3-dimensional visualization of the captured region.

With the aim to reduce the workload of the healthcare services, the development of computer-aided diagnosis systems (CAD) is very relevant (Doi, 2007). To do so, in the last years, the deep learning strategies have emerged as powerful techniques to solve medical imaging problems very effectively (Suzuki, 2017). However, there are some challenges to tackle when dealing with image modalities as CT or chest X-ray. First of all, the inferior level of detail and quality of the chest X-ray images implies that find representative patterns of the pathological affectation is more difficult (aspect that is even more accused in the case of the captures provided by the portable chest X-ray devices). Secondly, in the case of the CT images, despite the higher quality and higher detail of the captures, the methods are inherently more

complex to develop. A CT image is a conjunction of different X-ray images that are captured with different angles. Then, this set of different captures can be merged to create a 3-dimensional representation, in this case, of the chest, where each X-ray capture represents a 2-dimensional slice. The difficulty of the analysis process mainly emerges from the fact that only certain slices are useful to perform a study of the affectation of the disease. Therefore, one part of the methodological proposal must be to remove all the slices that are useless for the process. Moreover, both biomedical image modalities are affected by the issue of data scarcity. Deep learning models need datasets with large-scale dimensionality to be trained and provide effective results. However, it is well-known that in many biomedical imaging domains, the data scarcity is a very important problematic to deal with. In the case of the COVID-19, that has emerged very recently in contrast with other common pulmonary diseases, the aspect of data scarcity is even more important.

In this chapter, we explore a methodology developed for the automatic COVID-19 screening using chest X-ray images captured using with portable devices, providing the expert clinicians an automatic tool to reduce their workload in the global pandemic. Due to the recently emergence of this disease, the available data used for training the classification models is scarce. To overcome that data scarcity, the methodology can be splitted in 2 different parts. The first step performs a synthetic image generation with the CycleGAN, an image translation model (*i.e.,* a model that can convert images from a source scenario to another different target scenario) considering 4 different configurations for the generative models: an Unet-128 (Unet with 7 downsampling blocks), Unet-256 (Unet with 8 downsampling blocks), ResNet-6 (ResNet with 6 residual blocks) and ResNet-9 (ResNet with 9 residual blocks). Then, this set of generated images is added to original dataset. For the second step of the methodology, the augmented dataset is used to train the screening model, while the test is performed using only original images. Apart from data scarcity, the screening models must deal with the lower quality and lower level of detail of the images provided by the portable chest X-ray devices, in contrast with the fixed machinery. The methodology proposed on that work provides a reliable and robust method for COVID-19 screening despite the mentioned issues.

This chapter is structured as follows: The Background section talks about the techniques that can be found on the state of the art for COVID-19 screening or related tasks using chest X-ray and chest CT images, as well as some works that develop methodologies for image generation as data augmentation strategies. The Synthetic Image Generation and COVID-19 Screening with The Augmented Dataset section describes the dataset used for the development of the reference work, the proposed methodology, the experimental validation design and the obtained results with their correspondent discussion. The Solutions and Recommendations section proposes some of the possible solutions to tackle the problematics that appeared during the progress of the developed methodology. The Future Research Directions talks about the possible directions that could be follow in the research line that is related with this chapter, as the applications of synthetic image generation for biomedical imaging analysis. Finally, in Conclusion, we talk about the most important facts extracted from the analyzed topic and the studied methodology.

BACKGROUND

As chest X-ray and CT imaging are useful to diagnose a variety of diseases, many efforts have been done to develop CAD systems able to help clinicians while using this kind of biomedical imaging modalities, using classical computer vision techniques and classical machine learning strategies. As reference, the work from (Kumar et al., 2014) obtains a set of features from Gabor filtering that are then used as input for a classification model, which in this case is a Support Vector Machine (Cortes & Vapnik, 1995), with the aim of distinguishing between normal and pulmonary edema. The contribution of (Novo et al., 2015) proposes the use of the central adaptive medialness (Krissian et al., 2000), which is a method for detecting

tubular structures in 3D images, for selecting lung nodule candidates on CT images. In another proposal (Novo et al., 2014), the authors used a dataset of thoracic CT images to perform a reliable lung segmentation using different region growing approaches, including the juxtapleural nodules. The work from (Yan et al., 2012) proposes the development of a methodology for the lung segmentation task using chest X-ray images with the support of landmarks learned from manual annotation. The proposal of (Gonçalves et al., 2017) extracts a set of features from a nodular image region that is used as the input of classical machine learning classifier methods as Support Vector Machines and k Nearest Neighbors (Hwang & Wen, 1998) to compute the malignancy likelihood of a lung nodule. In this case, the authors use the dataset Lung Image Database Consortium (Armato III et al., 2011), that is composed of both CT and chest X-ray images.

With regards to data scarcity, many contributions have addressed the possible approaches to tackle this very relevant problematic. The most conventional data augmentation techniques are based on applying trivial transformations on images as random rotations or translations, among many other possible kinds of transformations (Wang et al., 2017). However, these data augmentation strategies can be insufficient to represent the notable variability of a specific medical imaging domain. In the last years, many works have proposed the image generation as a powerful data augmentation technique. Particularly, the Generative Adversarial Networks (GANs) are one of the most used network architectures for image generation (Creswell et al., 2018). One specific GAN architecture is the Cycle Consistent Adversarial Network, often denoted as CycleGAN (Zhu et al., 2017). The CycleGAN is an image translation model which is able to convert images from a scenario A to its hypothetical version in a scenario B and vice versa. The motivation of using the CycleGAN in this problem is due to the fact that this model is able to deal with unpaired datasets, in contrast with other translation models that are specifically designed for paired data. In the context of the chest X-ray imaging, GAN models have been used to solve data scarcity problems in some specific cases. As reference, the work from (Zhang et al., 2020) uses a GAN to perform organ segmentation in chest X-ray images in an unsupervised manner. The contribution of (Xu et al., 2020) uses GANs to recover high resolution chest X-ray images from low resolution images in a super-resolution fashion. The work from (Malygina et al., 2019) demonstrates the use of the CycleGAN to improve the pathology prediction in several different scenarios as pneumonia or fibrosis. With regards to the topic of this chapter, the work from (Morís et al., 2021a) demonstrates the suitability of image translation in the context of the COVID-19 screening using images provided by portable chest X-ray devices.

In the case of the automatic screening using chest CT imaging datasets, there are relevant contributions of CAD systems to help clinicians in the diagnostic processes. As reference, the work from (Xie et al., 2019) uses deep learning for lung nodule classification in 2 different classes, benignant and malignant, obtaining an accuracy of 91.60% and an AUC of 95.70%. The contribution of (Shadmi et al., 2018) proposes a deep learning strategy for coronary calcium segmentation, an important biomarker to measure the severity of cardiovascular diseases. The proposal of (Li et al., 2019) is developing a method for a fast pneumotorax detection in chest CT images, obtaining a 100% of sensitivity and an 82.5% of specificity. There are also other works that propose methods for image generation, to improve the performance of the screening systems. As reference, the work from (Han et al., 2019) uses a deep model based on the GAN paradigm to generate synthetic chest CT images with lung nodules. On the other hand, with regards to the main topic of this chapter, there are also many interesting works that proposes methods for COVID-19 detection and image generation working with chest CT images. As reference, the work from (Zheng et al., 2020) uses weakly-supervised deep learning models to detect COVID-19 in chest CT images, obtaining a ROC AUC of 0.959. Furthermore, the work from (Acar et al., 2021) tackles the problem of data scarcity using a GAN architecture to improve the performance of the COVID-19 screening in chest CT images.

On the other hand, many contributions have addressed other important tasks directly or indirectly related with COVID-19 screening on chest X-ray datasets. As reference, the work from (Vidal et al., 2021) uses a transfer learning framework to reuse the knowledge extracted from other different and well-known domain with a great number of samples to adapt it to the COVID-19 chest X-ray imaging domain, where data is much more scarce, in order to perform a reliable lung segmentation. The work from (Basu et al., 2020) uses transfer learning to develop a reliable automatic COVID-19 screening method. The contribution of (Misra et al., 2020) uses an ensemble of 3 different ResNet pretrained models to classify in 3 different classes: Normal, Pneumonia and COVID-19. (De Moura, Novo, et al., 2020) developed a methodology to perform an automatic COVID-19 screening using publicly available data of chest X-ray imaging. The work of (De Moura, García, et al., 2020) proposes the use of a classification model for the COVID-19 screening, considering a dataset of chest X-ray images captured with portable devices. Moreover, the work of (Morís et al., 2021b) proves the utility of adding a novel set of synthetic images generated with the method proposed on the above-mentioned work from the same authors, to the original dataset in the context of the COVID-19 screening. A work from the same authors (Morís et al., 2021c) proves the potential of training with a larger amount of portable chest X-ray imaging data.

SYNTHETIC IMAGE GENERATION AND COVID-19 SCREENING WITH THE AUGMENTED DATASET

In order to develop this methodology, the authors used a portable chest X-ray imaging dataset provided by the Radiology Service of the Complexo Hospitalario Universitario de A Coruña (CHUAC). In this line, the authors used a private dataset provided by a local public hospital institution, the Complexo Hospitalario Universitario de A Coruña (CHUAC). This dataset is divided in 3 different classes: Normal, Pathological and COVID-19. The class Normal is composed of patients without signs of pulmonary affectation that, however, can present other kinds of pathologies. The class Pathological is composed of patients that present pulmonary affectation caused by pulmonary pathologies different from COVID-19, but with compatible symptomatology. Lastly, the COVID-19 class refers to all the genuine COVID-19 cases. Examples of these images for each class are depicted in Figure 1. The dataset is balanced as is composed of 240 Normal cases, 240 Pathological cases and 240 COVID-19 cases. The images have variable resolutions that can be 1523 X 1904, 1526 X 1753, 1526 X 1754, 1526 X 1910, 949 X 827, 950 X 827 and 950 X 833 pixels. Those images were provided by 2 different models of portable chest X-ray devices: the Agfa dr100E GE and the Optima Rx200.

Figure 1: Representative examples for each class of the dataset. (a) Normal sample. (b) Pathological sample. (c) COVID-19 sample.

With regards to the proposed methodology itself, that is schematically described in Figure 2, the process is divided in 2 different parts where the first part of the methodology is in charge of the synthetic image

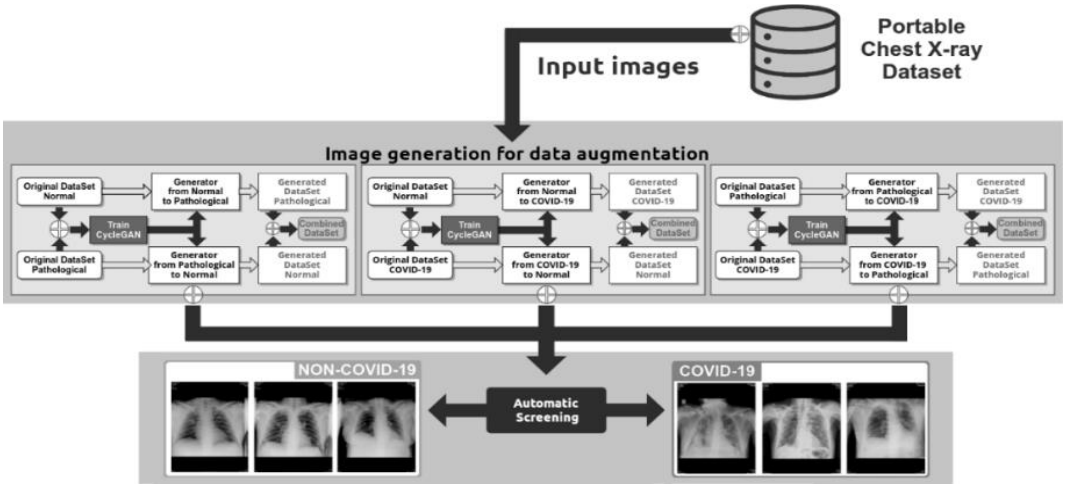

Figure 2: Overview of the methodology for data augmentation and COVID-19 screening using portable chest X-ray images. The first part performs the image generation while the second part performs the automatic COVID-19 Screening.

generation that is performed using an image translation model (and is described in detail in Subsection Image Generation for Data Augmentation) and where the second part of the methodology uses the novel set of synthetic images to artificially increase the size of the original input dataset (and is described in detail in Subsection Automatic Screening).

Image Generation for Data Augmentation

The CycleGAN is composed of 2 different generative models (G_{AB} and G_{BA}) and 2 different discriminative models (D_A and D_B). Its schematical representation can be seen in Figure 3. The model G_{AB} is trained to translate images from a domain A to its correspondent representation in domain B. On the other side, the model G_{BA} is trained to translate images from a domain B to a domain A. In addition, the discriminative model D_A is trained to distinguish original images from domain A and fake images generated by G_{BA} while the discriminative model D_B is trained to distinguish original images from domain B and fake images generated by G_{AB}. Therefore, the image translation is performed in 3 different scenarios: the first one converts from Normal to Pathological and vice versa, the second one converts from Normal to COVID-19 and vice versa while the third one converts from Pathological to COVID-19 and vice versa. Moreover, in the case of the considered reference work, authors used 4 different configurations for the generative model: Unet-128, Unet-256, ResNet-6 and ResNet-9 (those that were allowed by the CycleGAN original implementation). With regards to the discriminative models, a 70 X 70 PatchGAN is used as the architecture

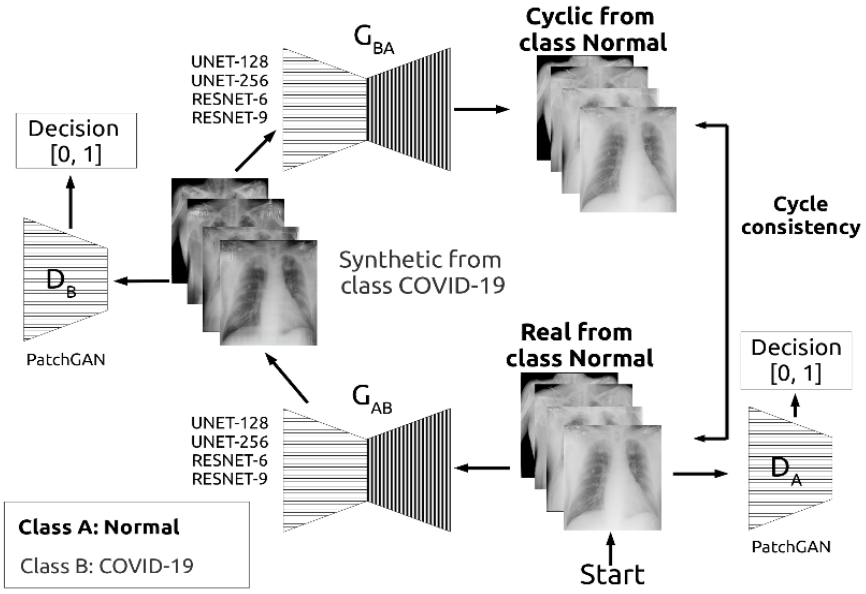

Figure 3: Overall description of the CycleGAN architecture for image generation. In this schematic representation, the class Normal is assumed as the domain A and the class COVID-19 is assumed as the class B.

in both cases. Thanks to the implementation of the CycleGAN, both generative and discriminative models are trained simultaneously for the 2 possible pathways on each case.

When all models are trained, G_{AB} and G_{BA} can be used to perform the image translations. Therefore, if we consider the class Normal as the domain A and the class Pathological as the domain B, the model G_{AB} is able to convert Normal images to their Pathological version while the model G_{BA} converts the Pathological images to their Normal version. The same idea applies for the other remaining 2 scenarios. The CycleGAN is complex to train, needing the definition of several different types of losses. With regards to this, there are 2 loss definitions: the adversarial loss and the cycle consistency loss. The adversarial loss is computed using the least-square loss to compare the predicted and the expected output. The expression of the adversarial loss is shown in Equation 1:

$$L_{GAN} = (G_{AB}, D_B, A, B) = E_{a \sim p_{data}(a)} \left[\left(D_B\left(G_{AB}(a)\right) - 1 \right)^2 \right] \quad (1)$$

where *a* denotes a particular original image that belongs to domain A and the generative model G_{AB} and the discriminative model D_B are used as reference,

In addition, the discriminative models must be trained to minimize the expression stated in Equation 2 taking the case of D_B as reference and considering b as an original image that belongs to domain B:

$$L_{GAN}(G_{AB}, D_B) = \frac{E_{a \sim p_{data}(a)}\left[\left(D_B(G_{AB})(a) \right)^2 \right] + E_{b \sim p_{data}(b)}\left[(D_B(b) - 1)^2 \right]}{2} \quad (2)$$

On the other hand, the model defines the cycle consistency loss. This expression adds 2 weight values, λ_A and λ_B. The weight value λ_A refers to the path that converts images from domain A to domain B and then to domain A again while the weight λ_B refers to the path that converts images from domain B to domain A and then to domain B again. The expression of the cycle consistency loss is stated in Equation 3:

$$L_{cyc}(G_{AB}, G_{BA}, \lambda_A, \lambda_B) = \lambda_A \cdot E_{a \sim p_{data}}(a)\left[||G_{BA}\left(G_{AB}(a)\right) - a||_1 \right]$$
$$+\lambda_B \cdot E_{b \sim p_{data}(b)}\left[||G_{AB}\left(G_{BA}(b)\right) - b||_1 \right] \quad (3)$$

Given an original image *a* from the domain A the idea of cycle consistency is that, if we convert that image to the domain B using the generative model G_{AB} and, afterwards, we use that output as the input of the generative model G_{BA} to convert the synthetic image from the domain B to the domain A, the final output image (denoted as Cycle A) must be the same as the original *a*. In other words, this means that *a* must be equal to Cycle A = $G_{BA}(G_{AB}(a))$.

Finally, the used implementation of the CycleGAN also uses another loss expression, which is known as identity loss. This loss value is used to prevent the model to perform undesired transformations on images. Given an image *a* from the domain *A*, the idea of identity loss is that, if we use that image as the input of the generative model G_{BA}, the model should obtain the same exact image (that can be denoted as idt_A). In other words, this means that a must be equal to idt_A = $G_{BA}(a)$. Considering all these aspects, the identity loss is expressed as can be seen in Equation 4.

$$L_{idt}(G_{AB}, G_{BA}, \lambda_A, \lambda_B) = E_{a \sim p_{data}(a)}[||G_{BA}(a) - a||_1]\lambda_A \cdot \lambda_{idt}$$
$$+E_{b \sim p_{data}(b)}[||G_{AB}(b) - b||_1] \cdot \lambda_B \cdot \lambda_{idt} \quad (4)$$

where λ_{idt} gives a weight value to the identity loss in the final objective expression. With all the loss functions defined, the joint expression is shown in Equation 5.

$$L(G_{AB}, G_{BA}, D_A, D_B, \lambda_A, \lambda_B, \lambda_{idt}) = L_{GAN}(G_{AB}, D_B, A, B) + L_{GAN}(G_{BA}, D_A, B, A)$$
$$+L_{cyc}(G_{AB}, G_{BA}, \lambda_A, \lambda_B) + L_{idt}(G_{AB}, G_{BA}, \lambda_A, \lambda_B, \lambda_{idt}) \quad (5)$$

Therefore, to update the networks weights, the expression defined in Equation 6 must be optimized:

$$G_{AB}^*, G_{BA}^* = arg \min_{G_{AB}, G_{BA}} \max_{D_A, D_B} L(G_{AB}, G_{BA}, D_A, D_B, \lambda_A, \lambda_B, \lambda_{idt}) \quad (6)$$

Other important training detail is that all the input images are resized to 256 X 256 X 3. Moreover, the CycleGAN models are all trained during 250 epochs with the Adam algorithm (Kingma & Ba, 2014) and a mini-batch size of 1. In terms of the optimization algorithm parameters, the authors use a constant value of learning rate of α=0.0002. Finally, an important aspect that must be noted is that all the images of the input dataset were used with the aim of training the CycleGAN models.

Automatic Screening

For the second part of the methodology, the new set of synthetic images is added to the training set of the COVID-19 screening. Therefore, the model is trained with a higher amount of data while the test is performed using only original images, in order to have a fair comparison against previous state of the art methods. The automatic COVID-19 screening is performed to prove 2 different hypotheses. First of all, it is used to measure the separability among the synthetic images generated for the 3 different above-mentioned scenarios (i.*e.*, Normal vs Pathological, Normal vs COVID-19 and Pathological vs COVID-19). The second hypothesis to prove is that using the novel set of synthetic images can improve the performance of the screening model.

In order to develop this COVID-19 screening method, the reference work adapts the training details designed for a previous approach. Particularly, for the classification task, authors use a Densely Connected Convolutional Network (DenseNet) as the network architecture (Huang et al., 2017), more precisely, a DenseNet-161. All screening models were trained during 200 epochs, optimizing with the Stochastic Gradient Descent Algorithm (SGD) (Ketkar, 2017) and a constant learning rate of $\alpha = 0.01$ with a first-order momentum of 0.9. Moreover, a mini-batch size of 4 was used, the input dataset is randomly splitted in 3 different sets, using a 60% of the samples for training, 20% of the samples for validation and the remaining 20 % of the samples for test and the training process is conducted 5 times. To have a global metric representative of the models behavior, given the values of the 5 repetitions, the mean and the standard deviation are obtained. Furthermore, the loss function used to train the screening model was the cross-entropy, which is defined in Equation 7:

$$L = -Y \cdot log\left(\hat{Y}\right) \quad (7)$$

Results and discussion

To validate the methodology, authors made a qualitative analysis of the generated synthetic images and they performed 5 different experiments with the automatic screening method as well as an additional sixth experiment, that are briefly described below:

- **1st experiment:** validates the separability between the class Normal and the class Pathological using only generated images.
- **2nd experiment:** performs the separability validation between the class Normal and the class COVID-19 using only generated images.
- **3rd experiment:** studies the separability between the class Pathological and the class COVID-19 using only generated images.
- **4th experiment:** the screening model is trained with the augmented dataset (composed of both original and generated images) but tested only with original images to separate between the class NON-COVID-19 (that merges the class Normal with the class Pathological) and the class COVID-19.
- **5th experiment:** ablation study to understand the behavior of the screening model given the number of generated images.

- **6th experiment:** qualitative analysis of the synthetic generated images.

To make the experimental validation, authors used metrics that are usually used in the state of the art. Denoting TP as True Positives, TN as True Negatives, FP as False Positives and FN as False Negatives, accuracy is expressed in Equation 8, recall is stated in Equation 9, precision is shown in Equation 10 and F1-Score can be seen in Equation 11.

$$Accuracy = \frac{TP+TN}{TP+FP+TN+FN} \quad (8)$$

$$Recall = \frac{TP}{TP+FN} \quad (9)$$

$$Precision = \frac{TP}{TP+FP} \quad (10)$$

$$F1 - Score = 2 \cdot \frac{Precision \cdot Recall}{Precision+Recall} \quad (11)$$

Moreover, authors complement the experimental validation with the correct classification and the misclassification ratios obtained from confusion matrices representative of each experiment and each generative model configuration.

1st Experiment: Separability Between Normal and Pathological (Only Generated Images)

Considering the test results of the first experiment (that validates the separability between the generated Normal samples and the generated Pathological samples), in terms of accuracy, the screening models obtain a 95.83%, 97.92%, 100.00% and 96.88% for each of the generative models configurations, respectively, Unet-128, Unet-256, ResNet-6 and ResNet-9. On the other hand, precision, recall and F1-Score of this first experiment are depicted in Figure 4. There, it can be seen that all metrics are equal or over 96% and, even in some cases, values are 100%, demonstrating the robustness of the method. Moreover, Figure 5 depicts the confusion matrices for the third experiment, where it can be seen that the correct classification ratios are satisfactory for both Normal class and Pathological class with all the 4 configurations, being higher or equal than 96% in all cases.

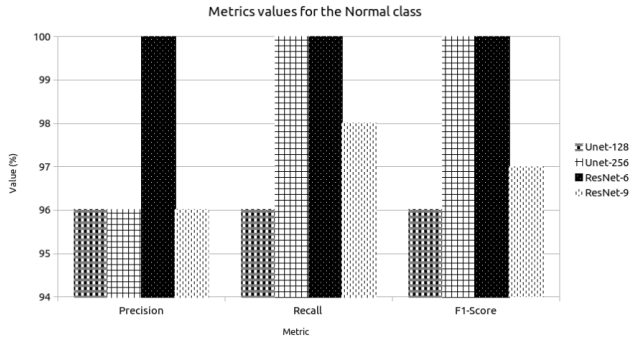

(a)

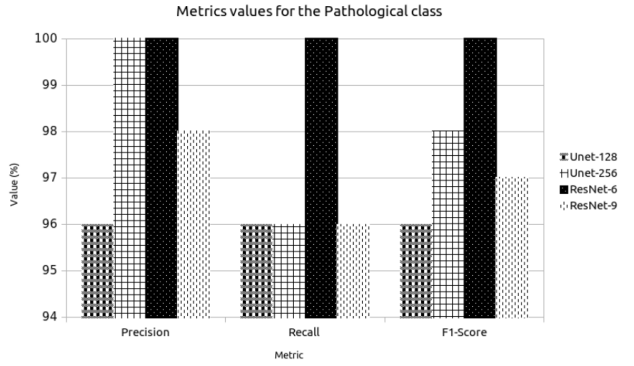

(b)

Figure 4: Metrics values in the case Normal vs Pathological (separability among generated images). (a) Values obtained for the Normal class. (b) Values obtained for the Pathological class.

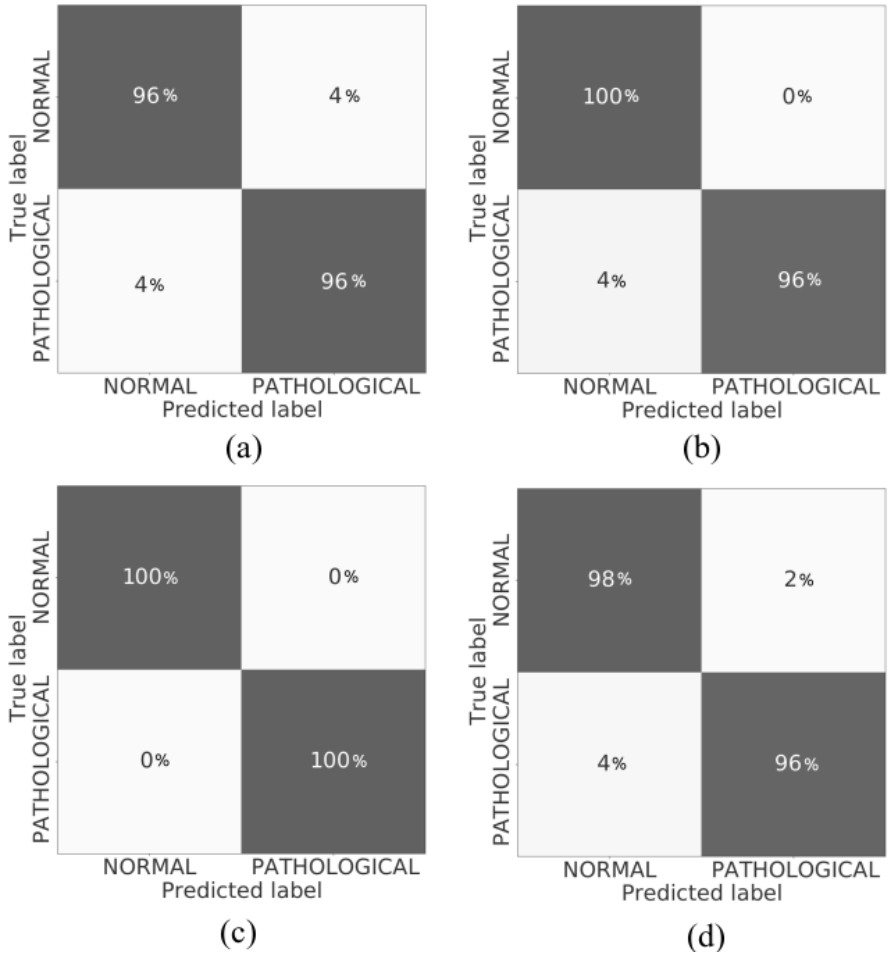

Figure 5: Confusion matrices of the 1st experiment given the 4 CycleGAN configurations that were selected. (a) Unet-128. (b) Unet-256. (c) ResNet-6. (d) ResNet-9.

2nd Experiment: Separability Between Normal and COVID-19 (Only Generated Images)

With regards to the test results of the second experiment, the separability between the Normal class and the COVID-19 class is proved, as it can be seen in Figure 6. In particular, once again, all values are close to 100%. The same happens with regards to the accuracy values and, in the same order as in the previous case, the screening models obtained a 94.79%, 100.00%, 96.88% and 96.88%. For this case, the confusion matrices are shown in Figure 7 where it can be seen that the correct classification ratio is always higher or equal than 94% for both classes and with all the configurations.

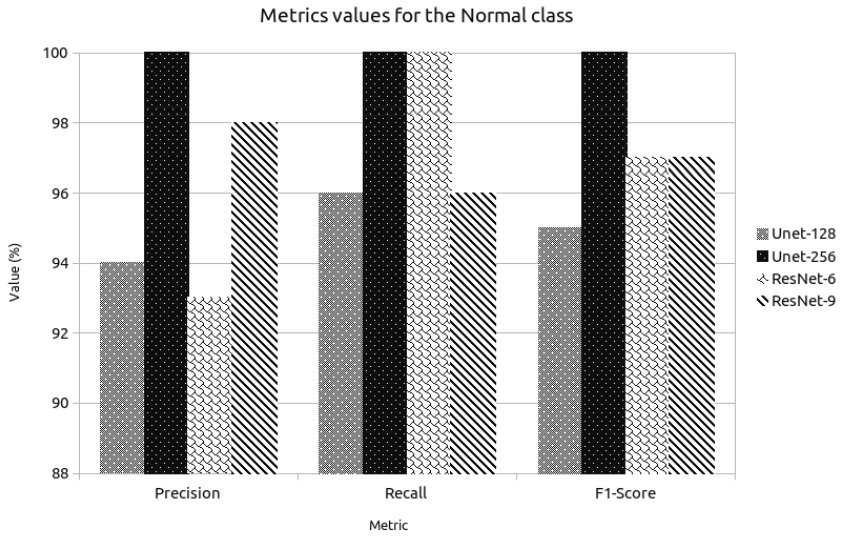

(a)

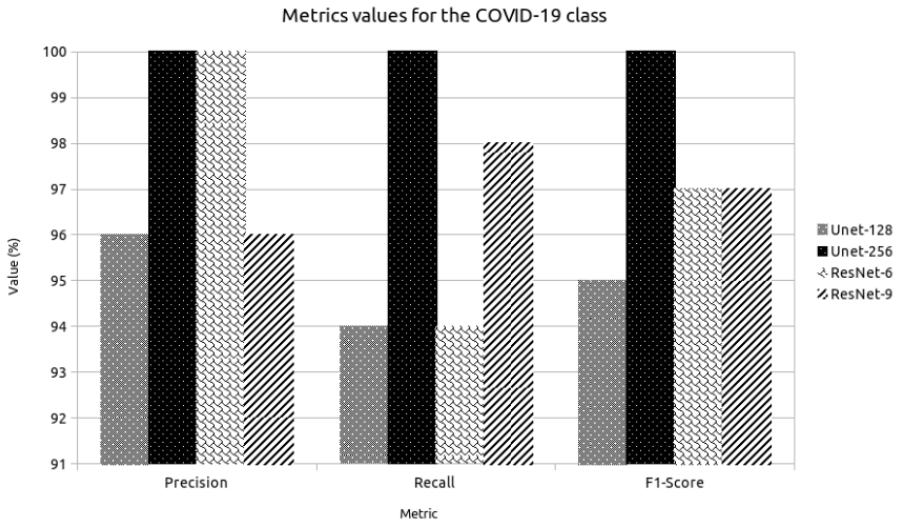

(b)

Figure 6: Metrics values in the case Normal vs COVID-19 (using only generated images). (a) Metrics values obtained for the Normal class. (b) Metrics values obtained for the COVID-19 class.

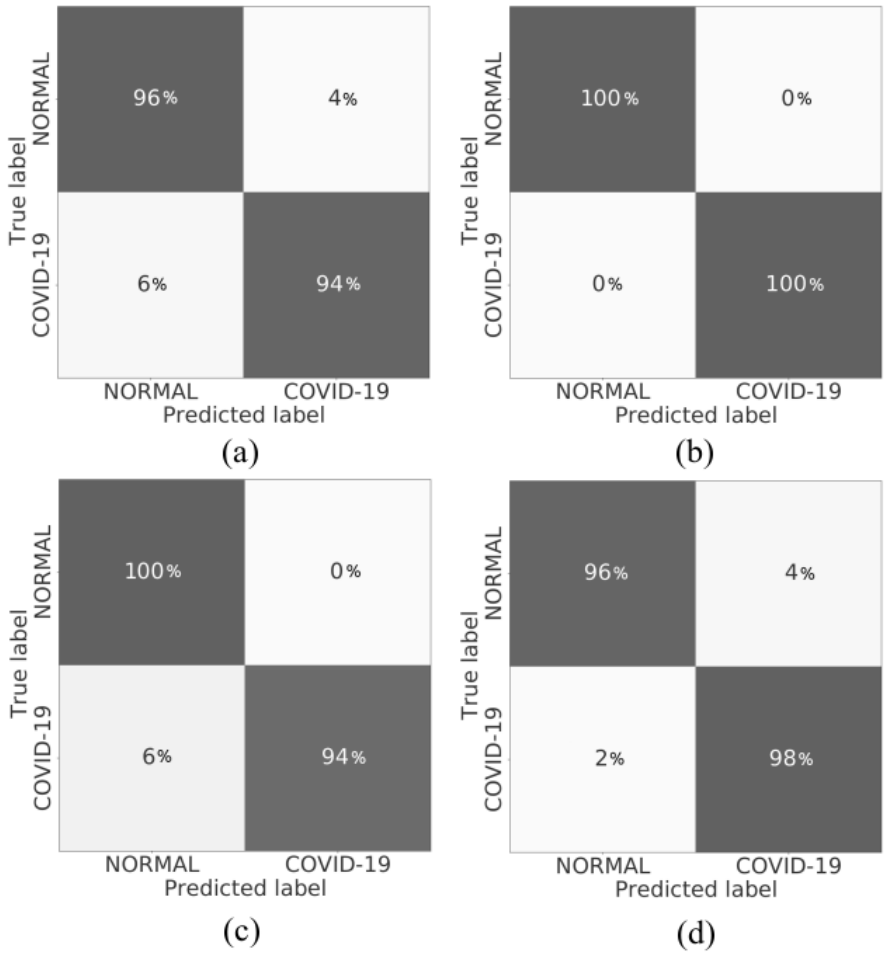

Figure 7: Confusion matrices results achieved during the 2nd experiment showing the 4 CycleGAN configurations that were chosen. (a) Unet-128. (b) Unet-256. (c) ResNet-6. (d) ResNet-9.

3rd Experiment: Separability Between Pathological and COVID-19 (Only Generated Images)

In terms of test results for the third experiment, Figure 8 has the metrics values for this experiment, showing that all cases are significantly close to 100% in a similar way as in the previous cases. Accuracy values have an identical behavior with a 98.96%, 100.00%, 97.92% and 100.00% considering the same order as in the previous cases. The confusion matrices that are shown in Figure 9 depict similar results as those seen in previous experiments. The correct classification ratios are significantly high for both classes and for all the 4 configurations considered for the image generation.

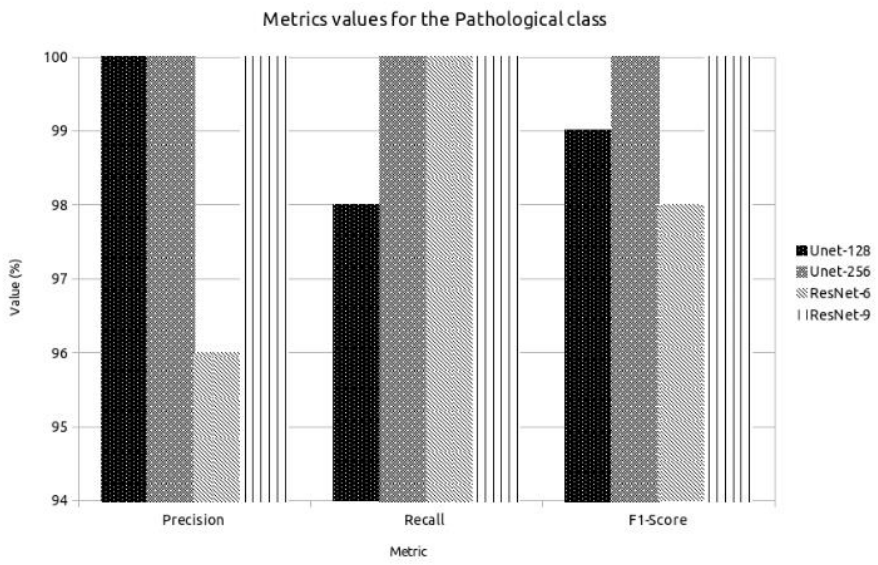

(a)

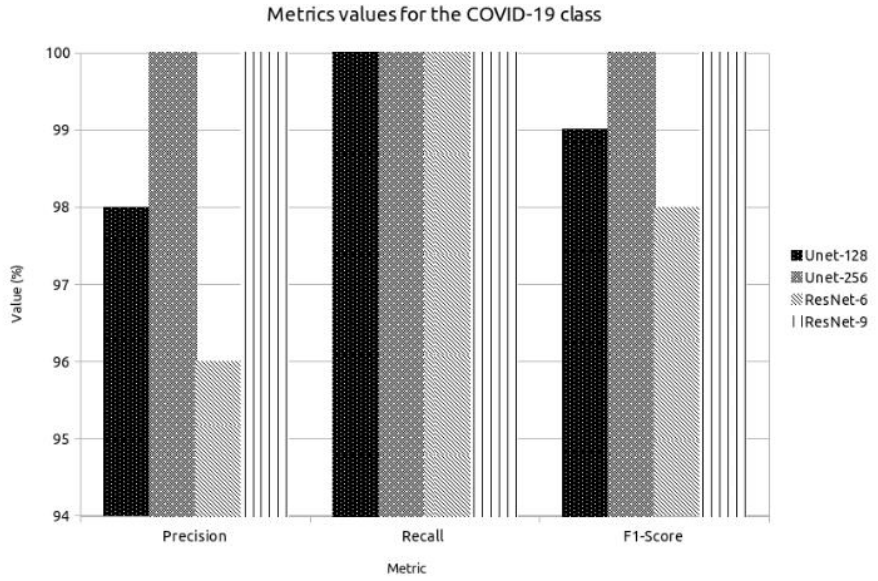

(b)

Figure 8: Metrics in the case Pathological vs COVID-19 (separability among generated images). (a) Normal class. (b) COVID-19 class.

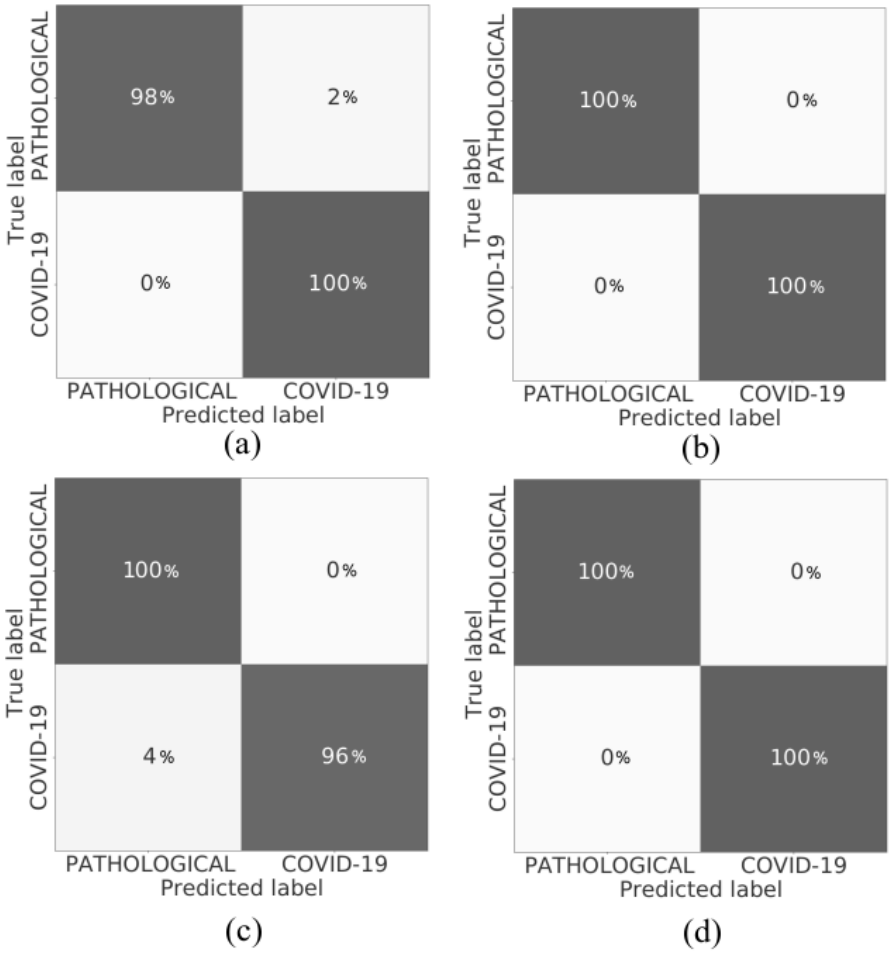

Figure 9: Confusion matrices results for the 3rd experiment with regards to the 4 CycleGAN configurations that were taken into account. (a) Unet-128. (b) Unet-256. (c) ResNet-6. (d) ResNet-9.

4th Experiment: Separability Between NON-COVID-19 and COVID-19 (Augmented Dataset)

Finally, the fourth experiment is the one that trains with the augmented dataset. In this experiment, the Normal class and the Pathological class are merged together to create a new NON-COVID-19 class, while the original COVID-19 class remains the same. For this last experiment, test results demonstrate that the automatic COVID-19 screening performed using the augmented dataset can obtain considerably acceptable results. The best effectiveness is obtained when generating the novel set of images configuring the generative model with the ResNet-9, obtaining an accuracy of 98.61%. More detailed results are shown in Figure 10, in terms of precision, recall and F1-Score. There it can be seen that, in an identical way as in the previous cases, all metrics are significantly close to 100%. Furthermore, in terms of correct classification ratios, values are higher or equal than 96% in all cases, for both classes and for all the considered configurations for image generation as it is shown in the confusion matrices of the Figure 11.

With respect to the previous contribution of (De Moura, García, et al., 2020) that proposes the same architectural and training details but without generating synthetic images, there is a significant improvement

from 90.27% to 98.61% in terms of accuracy. More detailed results can be seen in Figure 12 regarding recall, F1-Score and precision. For those results, it is remarkable the improvement in all metrics for both classes, but specially in the case of the COVID-19 class, as they improve from less than 90% to values considerably close to 100%.

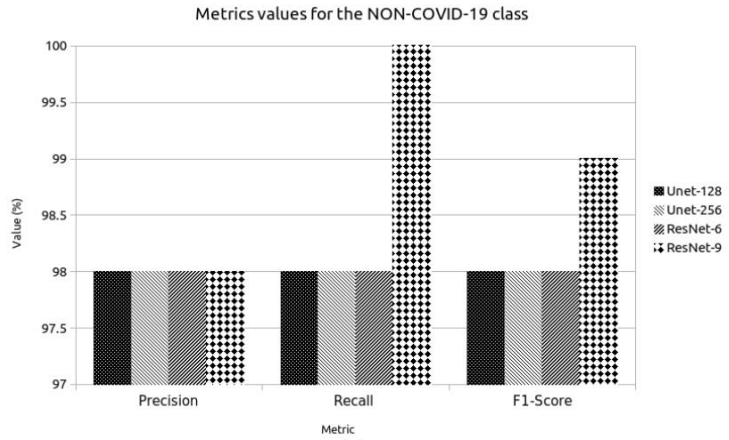

(a)

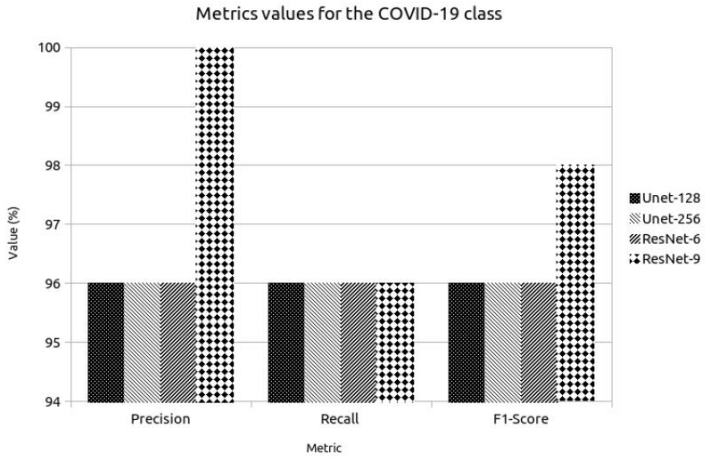

(b)

Figure 10: Metrics values in the case NON-COVID-19 vs COVID-19 (training with the augmented dataset and testing with only original images). (a) Values achieved in the case of the NON-COVID-19 class. (b) Values achieved in the case of the COVID-19 class.

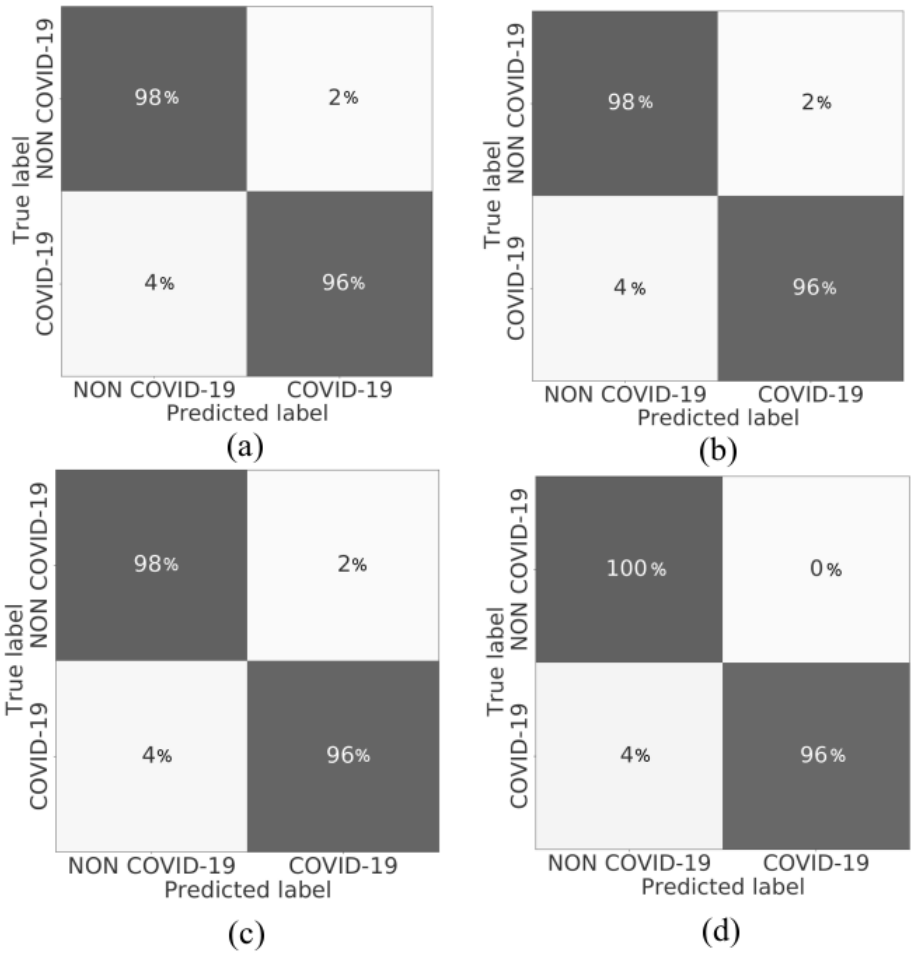

Figure 11: Confusion matrices results obtained during the 4th experiment with respect to the 4 CycleGAN configurations that were chosen for this work. (a) Unet-128. (b) Unet-256. (c) ResNet-6. (d) ResNet-9.

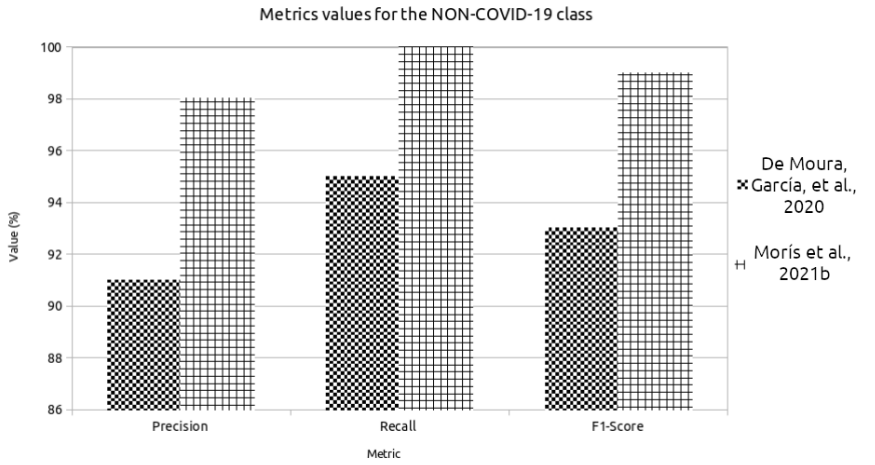

(a)

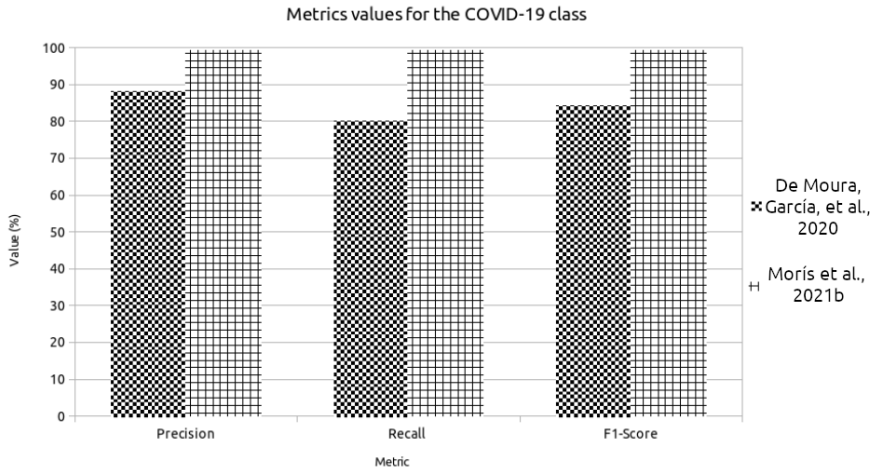

(b)

Figure 12: Metrics values comparison between 2 approaches: the screening with data augmentation (Morís et al., 2021b) and the screening without data augmentation (De Moura, García, et al., 2020). (a) Results in the case of the NON-COVID-19 class. (b) Results in the case of the COVID-19 class.

5th Experiment: Impact of the number of used generated images on the performance of the screening model

Moreover, authors conducted 5 additional experimental tests to prove the impact on the performance of the number of used generated images. In particular, they analyzed the performance while using the 0% of the whole set of generated images, the 20% (288 images), the 40% (576 images), the 60% (864 images), the 80% (1152 images) and the 100% (1440 images). To do this, they only considered 1 configuration for image generation, the ResNet-9, the one that achieved the best performance for the fourth experiment. The results, that can be seen in Figure 13, clearly show that performance increases when the number of synthetic images is higher, while it starts to converge at about the 80%.

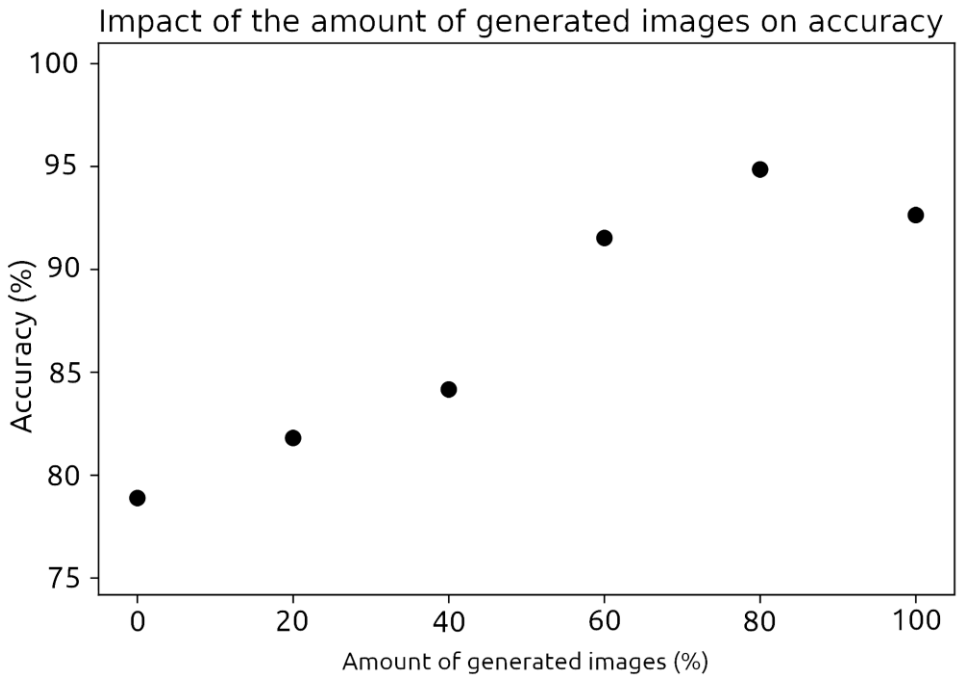

Figure 13: Impact of the number of synthetic images on the automatic screening effectiveness

6th Experiment: Qualitative Analysis of the Synthetic Generated Images

With regards to the synthetic image generation, the image translation models are able to generate fully synthesized images with a realistic appearance and with representative patterns of the scenario that want to be modeled, as it can be seen in the examples depicted in Figure 14. The difference images show that the most remarkable differences are noticed in pulmonary regions. Thus, as models are able to recognize the most remarkable patterns of each class, they can compute the differences to have a proper representation of the image in the target domain. Once the novel set of generated images is available, it can be added to a small size dataset, to increase its dimensionality and improve the performance that the deep models could achieve training with that artificially augmented dataset.

Therefore, the method is able to not only generate realistic chest X-ray images, but also to generate useful samples for clinical uses without paired data. Moreover, the great differences in the pulmonary regions, which are the most important areas of the images representative of the disease affectation, demonstrate that the method is focused on clinical criteria rather than other possible artifacts or irrelevant regions of the images for the diagnostic process.

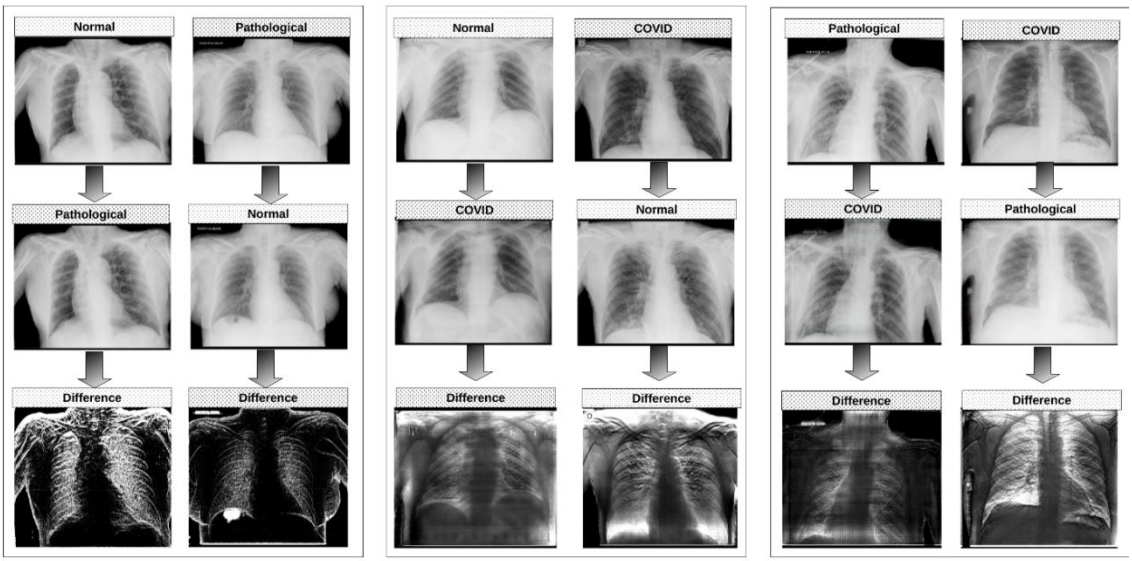

Figure 14: Examples of generated images and the differences between the generated and the original version for the 3 different scenarios (Normal vs Pathological, Normal vs COVID-19 and Pathological vs COVID-19)

SOLUTIONS AND RECOMMENDATIONS

The proposed methods for image generation have some problems that could be tackled to improve the performance of the screening models. As is stated on the content of this chapter, the portable chest X-ray devices provide images with lower quality, aspect that could be mitigated with several techniques such as the super resolution to resize original images to a higher resolution without losing quality or other classical enhancement strategies. Other interesting approach would be to train an image translation model to convert images from portable devices to their hypothetical version if they were captured with fixed machinery, to improve their quality. On the other hand, to help models to focus on the most important parts of the input images, an interesting approach would be to apply a ROI mask for images to only obtain the pulmonary regions. Furthermore, authors specified that they use a resolution of 256 X 256 X 3, which is considerably small. This makes the development of automatic screening methods more challenging and especially in this case, as the resolution of the chest X-ray images is very important because the pathological affectation must be explored looking at the fine details.

Apart from these challenges, many chest X-ray images from this kind of datasets show artifacts related with elements that are placed on patients to do the captures, elements that are placed on patients due to their condition (like the tubes that most critical patients need for mechanical ventilation), as well as other artifacts such as implants or other foreign objects that can appear on images. An approach to tackle this problem is to remove those elements from images. In the same way, as the important elements related with COVID-19 affectation can be detected on lung regions, bones suppression on images can be very useful.

FUTURE RESEARCH DIRECTIONS

Data scarcity is a challenging and well-known problem in the domain of biomedical imaging, not only for COVID-19 but also for many image modalities and for an important diversity of pathologies, especially when trying to train deep learning models, that need great amounts of data. Many efforts have been done in the direction of overcoming this data scarcity, developing several strategies as the application of traditional data augmentation techniques (such as random translations, rotations and other kind of linear and non-linear transformations), the transfer learning, the multi-task learning, the self-supervised learning or the weak supervised learning, among many others. In the last years, the focus has also been put on synthetic image generation, a powerful technique to artificially augment the size of the datasets, mitigating the data scarcity problem.

The Generative Adversarial Networks (GANs) have been often used for image generation in recent contributions. However, most of the GAN implementations are initially tested on broad domain image datasets. Therefore, their strength dealing with biomedical imaging problems is less frequently proved. Nevertheless, this chapter shows that are some interesting works that deal with this problematic. In particular, for the topic of this chapter, they demonstrate that image generation is a powerful data augmentation to overcome data scarcity in the domain of the COVID-19 when using image modalities as the CT or the chest X-ray, even with low quality images. Thus, the most probable future research directions are focused on developing and proving the strength of image generation methods to overcome data scarcity in specific biomedical imaging domains, different from those described in this chapter and applied to a great variety of diseases.

On the other hand, as it is well-known, in contrast with a broad domain, a particular biomedical imaging domain always represents the similar reality. This means that models can learn better from the reality they are looking at, presumably obtaining greater results. Furthermore, in the context of GANs applied to biomedical imaging, the image translation models are very relevant, especially those that can be trained without paired and registered data, as this kind of data is usually difficult to retrieve.

CONCLUSION

The COVID-19 disease has represented a great challenge for the whole humanity. Many efforts have been done to develop useful tools to tackle the dramatic situation of the healthcare services. One of the most important parts to mitigate the expansion of the pathogen that causes the COVID-19 is the early diagnose and the assessment of the evolution of the disease. There are several techniques to do so but, as the main affectation provoked by the coronavirus SARS-CoV-2 is located at the pulmonary regions, biomedical image modalities as chest X-ray are very useful to understand the severity of the disease on each moment. Chest X-ray imaging is a cheap and easy to perform diagnosis technique that allows clinicians to visualize the captured regions and, therefore, analyze the patterns that can be representative of different types of diseases. In the case of the COVID-19, considering the importance of cutting the chains of transmission, the decontamination of chest X-ray devices is a critical aspect. In that sense, the portable chest X-ray devices provide an alternative to fixed machinery, as they are easier to decontaminate.

The CAD systems have shown their utility in the last decades and specially in the last years with the raise of novel powerful strategies for biomedical imaging analysis. Particularly, the contributions of machine learning and, more precisely, the contributions of deep learning are remarkable in this field. These models are able to perform complex tasks directly dealing with raw data. During the COVID-19 pandemic, this

kind of systems are helpful for the clinicians to alleviate their workload, providing an automatic tool that also mitigates the subjectivity of the human experts. With regards to the chest X-ray image modality, deep models are able to directly deal with images of patients with suspected COVID-19 and extract the patterns that can conclude if that sample presents COVID-19 affectation or not, in a fully automatic way.

In this chapter, we analyzed the proposals of methods for portable chest X-ray image generation to improve the COVID-19 screening. To do so, we have taken into account a representative work from the state of the art. In that work, the methodology is splitted in 2 different modules. The first module generates the synthetic images using a CycleGAN architecture and considering 4 different configurations for the generative models. The CycleGAN architecture is used to do an image translation that can convert images from a source scenario to another target scenario. For the specific case of the reference work, the input dataset has 3 different classes: Normal, Pathological and COVID-19. Therefore, the translations are performed in 3 different contexts: the context where Normal images are converted to their Pathological version and vice versa, the context where Normal images are converted to their COVID-19 version and vice versa, and the context where Pathological images are converted to their COVID-19 representation and vice versa. This novel set is characterized of having synthetic images very similar to real chest X-ray captures and representative of the variability of the domain. Thus, this means that image generation represents a more powerful strategy in comparison with the classical data augmentation techniques.

For the second part of the methodology, an automatic COVID-19 screening is performed. This part of the methodology is developed using a DenseNet-161 architecture as the classification model. To prove the separability among the generated images, authors performed 3 different experiments, one for each translation scenario. Therefore, the first experiment is performed to validate the separability between the Normal and the Pathological class, the second experiment is performed to validate the separability between the Normal and the COVID-19 class and the third experiment is performed to validate the separability between the Pathological and the COVID-19 class. While these experiments are solely conducted using synthetic images, authors performed a fourth experiment using both original and synthetic images for training. In this case, they merge the Normal and the Pathological class to create a novel NON-COVID-19 class while the original COVID-19 class remains as the new COVID-19 class. To make a fair comparison with previous state of the art methods, they only add the novel set of generated samples in the training set. Therefore, the test is only performed with original images. Results show that there is a satisfactory separability between the generated images for all the considered scenarios. Furthermore, the fourth experiment proves that adding the novel set of synthetic images is useful to improve the automatic COVID-19 screening, obtaining an accuracy of 98.61% in contrast with the previous state of the art approach that only obtained a 90.27%. A fifth experiment was conducted to understand the impact of the number of generated images on the screening performance demonstrating that the effectiveness gets better when the amount of generated images is bigger. Finally, the sixth experiment performs the qualitative analysis of the generated synthetic images.

ACKNOWLEDGMENT

This research was funded by Instituto de Salud Carlos III, Government of Spain, [grant number DTS18/00136]; Ministerio de Ciencia e Innovación y Universidades, Government of Spain, [grant number RTI2018-095894-B-I00]; Ministerio de Ciencia e Innovación, Government of Spain through the research project with [grant number PID2019-108435RB-I00]; Consellería de Cultura, Educación e Universidade, Xunta de Galicia through the predoctoral and postdoctoral grant

contracts [grant number ED481A 2021/196] and [grant number ED481B 2021/059], respectively; and Grupos de Referencia Competitiva, [grant number ED431C 2020/24]; Axencia Galega de Innovación (GAIN), Xunta de Galicia, [grant number IN845D 2020/38]; CITIC, Centro de Investigación de Galicia [grant number ED431G 2019/01], receives financial support from Consellería de Educación, Universidade e Formación Profesional, Xunta de Galicia, through the ERDF (80%) and Secretaría Xeral de Universidades (20%).

REFERENCES

Acar, E., Şahin, E., & Yılmaz, İ. (2021). Improving effectiveness of different deep learning-based models for detecting COVID-19 from computed tomography (CT) images. Neural Computing and Applications, 1–21.

Armato III, S. G., McLennan, G., Bidaut, L., McNitt-Gray, M. F., Meyer, C. R., Reeves, A. P., Zhao, B., Aberle, D. R., Henschke, C. I., Hoffman, E. A., Kazerooni, E. A., MacMahon, H., van Beek, E. J. R., Yankelevitz, D., Biancardi, A. M., Bland, P. H., Brown, M. S., Engelmann, R. M., Laderach, G. E., … Clarke, L. P. (2011). The Lung Image Database Consortium (LIDC) and Image Database Resource Initiative (IDRI): A Completed Reference Database of Lung Nodules on CT Scans. Medical Physics, 38(2), 915–931. https://doi.org/10.1118/1.3528204

Basu, S., Mitra, S., & Saha, N. (2020). Deep Learning for Screening COVID-19 using Chest X-Ray Images. 2020 IEEE Symposium Series on Computational Intelligence (SSCI), 2521–2527. https://doi.org/10.1109/SSCI47803.2020.9308571

Ciotti, M., Ciccozzi, M., Terrinoni, A., Jiang, W.-C., Wang, C.-B., & Bernardini, S. (2020). The COVID-19 pandemic. Critical Reviews in Clinical Laboratory Sciences, 57(6), 365–388. https://doi.org/10.1080/10408363.2020.1783198

Coronavirus Resource Center, Johns Hopkins. (2020). COVID-19 Dashboard by the Center for Systems Science and Engineering (CSSE) at John Hopkins University. In ArcGIS Dashboards.

Cortes, C., & Vapnik, V. (1995). Support vector machine. Machine Learning, 20(3), 273–297.

Creswell, A., White, T., Dumoulin, V., Arulkumaran, K., Sengupta, B., & Bharath, A. A. (2018). Generative adversarial networks: An overview. IEEE Signal Processing Magazine, 35(1), 53–65.

De Moura, J., García, L. R., Vidal, P. F. L., Cruz, M., López, L. A., Lopez, E. C., Novo, J., & Ortega, M. (2020). Deep Convolutional Approaches for the Analysis of COVID-19 Using Chest X-Ray Images From Portable Devices. IEEE Access, 8, 195594–195607. https://doi.org/10.1109/ACCESS.2020.3033762

De Moura, J., Novo, J., & Ortega, M. (2020). Fully automatic deep convolutional approaches for the analysis of Covid-19 using chest X-ray images. MedRxiv, 2020.05.01.20087254. https://doi.org/10.1101/2020.05.01.20087254

Doi, K. (2007). Computer-aided diagnosis in medical imaging: Historical review, current status and future potential. Computerized Medical Imaging and Graphics, 31(4–5), 198–211.

Fiszman, M., Chapman, W. W., Aronsky, D., Evans, R. S., & Haug, P. J. (2000). Automatic detection of acute bacterial pneumonia from chest X-ray reports. Journal of the American Medical Informatics Association, 7(6), 593–604.

Gonçalves, L., Novo, J., Cunha, A., & Campilho, A. (2017). Learning Lung Nodule Malignancy Likelihood from Radiologist Annotations or Diagnosis Data. Journal of Medical and Biological Engineering, 38. https://doi.org/10.1007/s40846-017-0317-2

Han, C., Kitamura, Y., Kudo, A., Ichinose, A., Rundo, L., Furukawa, Y., Umemoto, K., Li, Y., & Nakayama, H. (2019). Synthesizing Diverse Lung Nodules Wherever Massively: 3D Multi-Conditional GAN-Based CT Image Augmentation for Object Detection. 2019 International Conference on 3D Vision (3DV), 729–737. https://doi.org/10.1109/3DV.2019.00085

Hayden, G. E., & Wrenn, K. W. (2009). Chest radiograph vs. Computed tomography scan in the evaluation for pneumonia. The Journal of Emergency Medicine, 36(3), 266–270.

Huang, G., Liu, Z., & Weinberger, K. Q. (2017). Densely Connected Convolutional Networks. 2017 IEEE Conference on Computer Vision and Pattern Recognition (CVPR), 2261–2269.

Hwang, W.-J., & Wen, K.-W. (1998). Fast kNN classification algorithm based on partial distance search. Electronics Letters, 34(21), 2062–2063.

Jacobi, A., Chung, M., Bernheim, A., & Eber, C. (2020). Portable chest X-ray in coronavirus disease-19 (COVID-19): A pictorial review. Clinical Imaging, 64, 35–42.

Ketkar, N. (2017). Stochastic Gradient Descent. In Deep Learning with Python: A Hands-on Introduction (pp. 113–132). Apress. https://doi.org/10.1007/978-1-4842-2766-4_8

Kingma, D. P., & Ba, J. (2014). Adam: A method for stochastic optimization. ArXiv Preprint ArXiv:1412.6980.

Kooraki, S., Hosseiny, M., Myers, L., & Gholamrezanezhad, A. (2020). Coronavirus (COVID-19) Outbreak: What the Department of Radiology Should Know. Journal of the American College of Radiology, 17(4), 447–451. https://doi.org/10.1016/j.jacr.2020.02.008

Krissian, K., Malandain, G., Ayache, N., Vaillant, R., & Trousset, Y. (2000). Model-Based Detection of Tubular Structures in 3D Images. Computer Vision and Image Understanding, 80(2), 130–171. https://doi.org/10.1006/cviu.2000.0866

Kumar, A., Wang, Y.-Y., Liu, K.-C., Tsai, I.-C., Huang, C.-C., & Hung, N. (2014). Distinguishing normal and pulmonary edema chest x-ray using Gabor filter and SVM. 2014 IEEE International Symposium on Bioelectronics and Bioinformatics (IEEE ISBB 2014), 1–4. https://doi.org/10.1109/ISBB.2014.6820918

Li, X., Thrall, J. H., Digumarthy, S. R., Kalra, M. K., Pandharipande, P. V., Zhang, B., Nitiwarangkul, C., Singh, R., Khera, R. D., & Li, Q. (2019). Deep learning-enabled system for rapid pneumothorax screening on chest CT. European Journal of Radiology, 120, 108692. https://doi.org/10.1016/j.ejrad.2019.108692

Malygina, T., Ericheva, E., & Drokin, I. (2019). Data Augmentation with GAN: Improving Chest X-Ray Pathologies Prediction on Class-Imbalanced Cases. International Conference on Analysis of Images, Social Networks and Texts, 321–334.

Misra, S., Jeon, S., Lee, S., Managuli, R., Jang, I.-S., & Kim, C. (2020). Multi-Channel Transfer Learning of Chest X-ray Images for Screening of COVID-19. Electronics, 9(9). https://doi.org/10.3390/electronics9091388

Morís, D. I., de Moura, J., Novo, J., & Ortega, M. (2021a). Cycle Generative Adversarial Network Approaches to Produce Novel Portable Chest X-Rays Images for Covid-19 Diagnosis. ICASSP 2021-2021 IEEE International Conference on Acoustics, Speech and Signal Processing (ICASSP), 1060–1064.

Morís, D. I., de Moura Ramos, J. J., Buján, J. N., & Hortas, M. O. (2021b). Data augmentation approaches using cycle-consistent adversarial networks for improving COVID-19 screening in portable chest X-ray images. Expert Systems with Applications, 185, 115681.

Morís, D. I., Moura, J. de, Novo, J., & Ortega, M. (2021c). Comprehensive Analysis of the Screening of COVID-19 Approaches in Chest X-ray Images from Portable Devices. European Symposium on Artificial Neural Networks (ESANN 2021), 165–170.

Novo, J., Gonçalves, L., Mendonça, A. M., & Campilho, A. (2015). 3D lung nodule candidate detection in multiple scales. 2015 14th IAPR International Conference on Machine Vision Applications (MVA), 61–64. https://doi.org/10.1109/MVA.2015.7153133

Novo, J., Rouco, J., Mendonça, A., & Campilho, A. (2014). Reliable Lung Segmentation Methodology by Including Juxtapleural Nodules. 8815, 227–235. https://doi.org/10.1007/978-3-319-11755-3_26

Puderbach, M., Eichinger, M., Haeselbarth, J., Ley, S., Kopp-Schneider, A., Tuengerthal, S., Schmaehl, A., Fink, C., Plathow, C., Wiebel, M., & others. (2007). Assessment of morphological MRI for pulmonary changes in cystic fibrosis (CF) patients: Comparison to thin-section CT and chest x-ray. Investigative Radiology, 42(10), 715–724.

Shadmi, R., Mazo, V., Bregman-Amitai, O., & Elnekave, E. (2018). Fully-convolutional deep-learning based system for coronary calcium score prediction from non-contrast chest CT. 2018 IEEE 15th International Symposium on Biomedical Imaging (ISBI 2018), 24–28. https://doi.org/10.1109/ISBI.2018.8363515

Suzuki, K. (2017). Overview of deep learning in medical imaging. Radiological Physics and Technology, 10(3), 257–273.

Tahamtan, A., & Ardebili, A. (2020). Real-time RT-PCR in COVID-19 detection: Issues affecting the results. Expert Review of Molecular Diagnostics, 20(5), 453–454. https://doi.org/10.1080/14737159.2020.1757437

Van Cleeff, M., Kivihya-Ndugga, L., Meme, H., Odhiambo, J., & Klatser, P. (2005). The role and performance of chest X-ray for the diagnosis of tuberculosis: A cost-effectiveness analysis in Nairobi, Kenya. BMC Infectious Diseases, 5(1), 1–9.

Vidal, P. F., de Moura, J., Novo, J., & Ortega, M. (2021). Multi-stage transfer learning for lung segmentation using portable X-ray devices for patients with COVID-19. Expert Systems with Applications, 173, 114677. https://doi.org/10.1016/j.eswa.2021.114677

Wang, J., Perez, L., & others. (2017). The effectiveness of data augmentation in image classification using deep learning. Convolutional Neural Networks Vis. Recognit, 11, 1–8.

Wei, J., Hagihara, Y., Shimizu, A., & Kobatake, H. (2002). Optimal image feature set for detecting lung nodules on chest X-ray images. In CARS 2002 computer assisted radiology and surgery (pp. 706–711). Springer.

Xie, Y., Xia, Y., Zhang, J., Song, Y., Feng, D., Fulham, M., & Cai, W. (2019). Knowledge-based Collaborative Deep Learning for Benign-Malignant Lung Nodule Classification on Chest CT. IEEE Transactions on Medical Imaging, 38(4), 991–1004. https://doi.org/10.1109/TMI.2018.2876510

Xu, L., Zeng, X., Huang, Z., Li, W., & Zhang, H. (2020). Low-dose chest X-ray image super-resolution using generative adversarial nets with spectral normalization. Biomedical Signal Processing and Control, 55, 101600. https://doi.org/10.1016/j.bspc.2019.101600

Yan, Z., Zhang, J., Zhang, S., & Metaxas, D. N. (2012). Automatic rapid segmentation of human lung from 2D chest X-ray images. Proc. of MICCAI Workshop on Sparsity Techniques in Medical Imaging.

Zhang, Y., Miao, S., Mansi, T., & Liao, R. (2020). Unsupervised X-ray image segmentation with task driven generative adversarial networks. Medical Image Analysis, 62, 101664. https://doi.org/10.1016/j.media.2020.101664

Zheng, C., Deng, X., Fu, Q., Zhou, Q., Feng, J., Ma, H., Liu, W., & Wang, X. (2020). Deep learning-based detection for COVID-19 from chest CT using weak label. MedRxiv.

Zhu, J.-Y., Park, T., Isola, P., & Efros, A. A. (2017). Unpaired image-to-image translation using cycle consistent adversarial networks. Proceedings of the IEEE International Conference on Computer Vision, 2223–2232.

ADDITIONAL READING

Alghamdi, H. S., Amoudi, G., Elhag, S., Saeedi, K., & Nasser, J. (2021). Deep Learning Approaches for Detecting COVID-19 From Chest X-Ray Images: A Survey. *IEEE Access*, *9*, 20235–20254. doi:10.1109/ACCESS.2021.3054484

Fatima, S., Ratnani, I., Husain, M., & Surani, S. (2020). Radiological Findings in Patients with COVID-19. *Cureus*, *12*(4), e7651. https://doi.org/10.7759/cureus.7651

Fusco, R., Grassi, R., Granata, V., Setola, S. V., Grassi, F., Cozzi, D., … Petrillo, A. (2021). Artificial Intelligence and COVID-19 Using Chest CT Scan and Chest X-ray Images: Machine Learning and Deep Learning Approaches for Diagnosis and Treatment. *Journal of Personalized Medicine*, *11*(10). doi:10.3390/jpm11100993

Hervella, Á. S., Rouco, J., Novo, J., & Ortega, M. (2020). Self-supervised multimodal reconstruction of retinal images over paired datasets. *Expert Systems with Applications*, *161*, 113674. doi:10.1016/j.eswa.2020.113674

Hervella, Á. S., Rouco, J., Novo, J., & Ortega, M. (2021). Chapter 15 - Multimodal reconstruction of retinal images over unpaired datasets using cyclical generative adversarial networks. In A. Solanki, A. Nayyar, & M. Naved (Reds), *Generative Adversarial Networks for Image-to-Image Translation* (bll 347–376). doi:10.1016/B978-0-12-823519-5.00014-2

Huang, S., Yang, J., Fong, S., & Zhao, Q. (2021). Artificial intelligence in the diagnosis of COVID-19: challenges and perspectives. *International journal of biological sciences*, *17*(6), 1581–1587. https://doi.org/10.7150/ijbs.58855

Lee, J. G., Jun, S., Cho, Y. W., Lee, H., Kim, G. B., Seo, J. B., & Kim, N. (2017). Deep learning in medical imaging: general overview. *Korean journal of radiology*, *18*(4), 570-584.

Yi, X., Walia, E., & Babyn, P. (2019). Generative adversarial network in medical imaging: A review. *Medical Image Analysis*, *58*, 101552. doi:10.1016/j.media.2019.101552

KEY TERMS AND DEFINITIONS

Chest X-ray: Medical image modality that allows to visualize the inside of the thoracic region of a patient using a low dose of ionic radiation.

Computer Aided Diagnosis: Systems that are developed to improve the comprehension of medical images and help clinicians to make decisions.

Computerized Tomography: Medical image modality that combines a set of X-ray slices to get a 3-dimensional representation of a particular studied region of the body.

Deep Learning: Type of machine learning strategies that allows to create powerful classification and regression models able to deal directly with raw data.

Image Translation: Algorithmic process that converts an image from a source domain to another different target domain (for example, convert the image of an orange to an image of an apple).

Portable X-ray Devices: X-ray capturing devices that can moved to where the patients are placed.

Screening: Medical strategy that performs a diagnostic test on people that are considered healthy a priori with the aim to detect a possible disease on its mild stages.